THE JOURNAL OF PHYSICAL CHEMISTRY C

Article

pubs.acs.org/JPCC

Nanostructured Ta_3N_5 Films as Visible-Light Active Photoanodes for Water Oxidation

Hoang X. Dang,[†] Nathan T. Hahn,[†] Hyun S. Park,[‡] Allen J. Bard,[‡] and C. Buddie Mullins*[,†,‡]

[†]Department of Chemical Engineering, and [‡]Department of Chemistry and Biochemistry, Center for Electrochemistry, Texas Materials Institute, and Center for Nano- and Molecular Science, University of Texas at Austin, 1 University Station C0400, Austin, Texas 78712-0231, United States

Supporting Information

ABSTRACT: Nanostructured Ta_3N_5 photoanodes (band gap of ~2.0 eV) were synthesized via a two-step process: first, nanocolumnar Ta_2O_5 films were deposited by evaporation of tantalum metal in a vacuum chamber in a low pressure oxygen ambient followed by heating in an ammonia gas flow to convert Ta_2O_5 into orthorhombic Ta_3N_5. Under Xe lamp irradiation (~73 mW/cm^2), a 100 nm nanoporous Ta_3N_5 electrode achieved an anodic photocurrent of ~1.4 mA/cm^2 at +0.5 V versus Ag/AgCl in 1 M KOH solution. By comparison, a dense film achieved ~0.4 mA/cm^2 clearly illustrating the importance of nanostructuring for improving the performance of Ta_3N_5 photoanodes. However, Ta_3N_5 films suffered from inherent self-oxidation under light illumination, and application of a cobalt cocatalyst layer was found to improve the stability as well as photocatalytic activity of the Ta_3N_5 films.

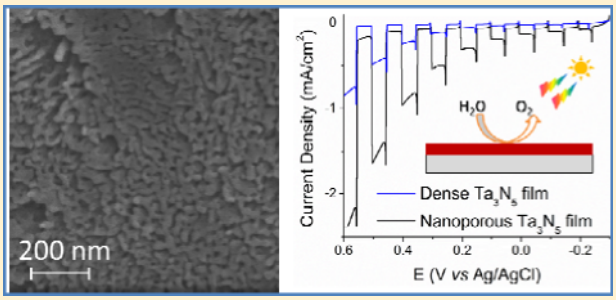

INTRODUCTION

Recent calculations show that using just a small fraction of the energy from the sunlight reaching our planet can meet the world energy demand.[1] However, it has proven to be extremely challenging to find ways to economically convert solar energy into usable forms. The cost-effective production of hydrogen fuel from sunlight and water is therefore considered one of the "Holy Grails" of chemistry.[2] One method is photoelectrochemical (PEC) water splitting using a photocatalyst. In a single-semiconductor, unbiased PEC system, catalyzing the water electrolysis process requires the material to have band edge positions (the top of the valence band and the bottom of conduction band) that straddle the water oxidation and proton reduction potentials while providing appropriate overpotentials for acceptable kinetics in driving the evolution of hydrogen and oxygen. In addition, to efficiently collect the incident sunlight energy, it is necessary that the band gap (E_g) of the material be narrow enough (E_g < 3.0 eV) to harvest a sizable fraction of the visible region of the solar spectrum.[3] Fujishima and Honda[4] first suggested the occurrence of water splitting in a Pt−TiO_2 electrochemical cell in 1972, and since this pioneering work there have been several studies regarding the synthesis and fabrication of long-lived, inexpensive photocatalysts that can utilize sunlight to produce hydrogen using water as the feed stock. However, these materials are either unstable or not sufficiently efficient.

Ta_3N_5 is a promising candidate as a photocatalyst for a single semiconductor system due to its visible-light absorption up to 600 nm ($E_g \approx 2.1$ eV), thermodynamically appropriate band edge positions for the water splitting process,[3,5−9] and its maximum theoretical photoconversion (AM 1.5 global solar illumination) of 15.9%.[10] There have been several studies on Ta_3N_5 particles as photocatalysts for hydrogen or oxygen evolution under visible light in the presence of sacrificial agents, but few studies evaluating the PEC performance of Ta_3N_5 thin films.[11−17] The fabrication and PEC performance of Ta_3N_5 films by a radio frequency sputtering technique[3] (dense films) or anodization[9] (nanotubular films) has been reported. However, from these studies, it is difficult to see whether nanostructuring is necessary to improve the PEC performance of Ta_3N_5. For this reason, we have employed a single technique to synthesize Ta_3N_5 films having either dense or porous structure to understand this difference.

Our growth of nanostructured Ta_3N_5 films for photoelectrocatalysis takes place via a two-step process: first, we grow porous Ta_2O_5 films by evaporation of tantalum metal in a vacuum chamber at a glancing angle with a low pressure ambient of oxygen (3×10^{-6} Torr of O_2) [this process is referred to as reactive ballistic deposition (RBD) at a glancing angle] followed by a nitridation step in a tube furnace containing an ammonia atmosphere. A key factor for synthesizing high surface area films via RBD is the limitation of adatom surface diffusion during film growth. For Ta_2O_5, when the growth surface is near room temperature (or below), surface diffusion is restrained and porous nanostructured surfaces can be generated. This growth process is described

Received: July 25, 2012
Revised: August 14, 2012
Published: August 15, 2012

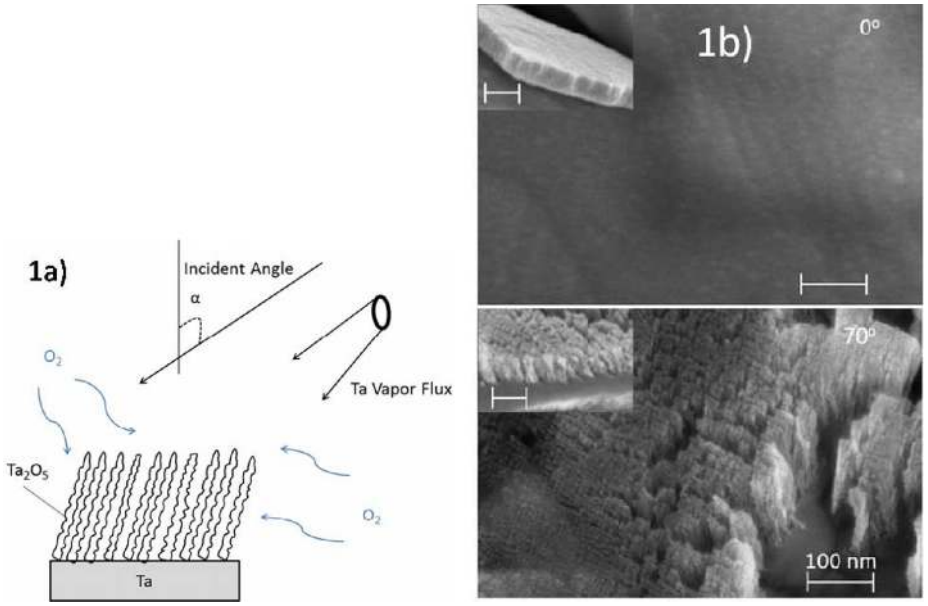

Figure 1. (a) Schematic of the reactive ballistic deposition (RBD) technique. Nanocolumnar Ta_2O_5 films are grown by evaporating Ta at a glancing angle on a Ta substrate in the presence of oxygen as the reactive gas. (b) SEM images of as-deposited Ta_2O_5 films on Ta foils at varying deposition angles: $\alpha = 0°$ (right, above) and 70° (right, bottom). All scale bars including the inset are 100 nm.

as "hit-and-stick" or ballistic deposition (BD).[18] In this scenario, vapor phase atoms or molecules travel from their source along straight-line trajectories to the deposition surface where they are incorporated in close proximity to their original landing sites.[18] At oblique angles of metal deposition, topographically elevated points, created stochastically during the initial growth, preferentially intercept the incoming vapor-phase atoms while shadowing lower regions.[19] This self-shadowing growth process can result in very porous nanocolumnar films. Brett et al.[20] have grown highly engineered and ordered films using ballistic deposition at glancing deposition angles to create arrays of micrometer-length nanocolumns, -zigzags, and -helices. This growth technique [without a reactive gas such as oxygen, ethylene, etc.] is sometimes referred to as glancing angle deposition (GLAD), and it has been the subject of two recent reviews by Abelmann and Lodder[19] as well as Hawkeye and Brett.[21]

The capabilities of ballistic deposition can be extended further via addition of a reactive ambient (O_2, C_2H_4, etc.) as described by Dohnálek and Kay in their pioneering paper.[22] By this method, metal-compound thin films are grown by reaction of the metallic adatoms and the adsorbed ambient gas. As suggested above, this technique is referred to as reactive ballistic deposition (RBD).[22,23] BD or RBD has been used to grow highly structured films from a wide variety of materials including Pd,[24] Cr,[25] Cu,[25] Fe,[26] Ti,[27] TiO_2,[28−31] Mn,[32] MgO,[22] Ta_2O_5,[33,34] WO_3,[33] SiO_X,[35,36] MgF_2,[32] CaF_2,[32] TiC,[37−39] and Fe_2O_3.[40,41] The resulting films often have optical, electronic, magnetic, and chemi-physical surface properties that can differ from dense, nonstructured films of similar composition. Detailed studies of RBD grown hematite,[40] Ti doped-hematite,[41] Si doped-hematite,[42] nanostructured $BiVO_4$,[43] and Mo and W incorporated nanostructured $BiVO_4$[44] films for photoelectrochemical applications have recently been reported. During the course of our investigation, we found that the Ta_3N_5 films suffered from serious photocorrosion while being tested in 1 M KOH, which was not reported earlier.[9] Interestingly, a simple cobalt surface treatment was found to improve the photocurrent stability as well as boost the PEC performance of the Ta_3N_5 films. The use of cobalt-based cocatalysts for various photoelectrodes[45−52] is promising due to the abundance of cobalt as compared to commonly used cocatalysts such as IrO_2 or Pt. Also, oxygen detection experiments were carried out to calculate the contribution of the actual water oxidation in the overall observed photocurrent of the Ta_3N_5 photoanodes.

EXPERIMENTAL SECTION

Film Preparation. RBD Ta_2O_5 films were deposited on Ta foil substrates at room temperature by evaporating tantalum metal in a background of O_2 (partial pressure of $O_2 \approx 3 \times 10^{-6}$ Torr) as a reactive gas under high vacuum conditions. Before film growth was started, the vacuum chamber was pumped to $\sim 5 \times 10^{-8}$ Torr. For a typical film synthesis, pieces of 1 cm × 2 cm Ta substrates were cut from a larger 25 μm thick Ta foil (99.95%, Alfa Aesar), and then sonicated in alcohol and acetone for ∼10 min each before being rinsed with deionized water. The Ta substrate was then dried in a gentle N_2 flow before loading on a substrate holder positioned within the vacuum chamber. A home-built evaporator was used to evaporate Ta from a 0.125 in. diameter Ta rod (3N8 purity, ESPI). The sample holder was ∼6 in. from the evaporating source and could be rotated to a target deposition angle, α, which is the angle between the direction normal to the Ta foil substrate and the evaporant flux (see Figure 1a for a schematic of the RBD technique). The evaporating tantalum flux was measured using a quartz crystal microbalance (QCM). From this flux value and the deposition angle, the deposition time required for a desired film thickness was determined. The chamber was then backfilled with O_2 gas (99.99%, Matheson) to $\sim 3 \times 10^{-6}$ Torr using a leak valve. Thermal nitridation in an ammonia environment of the as-deposited Ta_2O_5 films was carried out in a tube furnace (OTF-1200X, MTI) at temperatures ranging from 700 to 850 °C for 8 h. A gas flow controller (Alicat Scientific) was employed to control the rate of NH_3 gas (Anhydrous 99.99%, Matheson) flowing through a

dx.doi.org/10.1021/jp307369z | J. Phys. Chem. C 2012, 116, 19225−19232

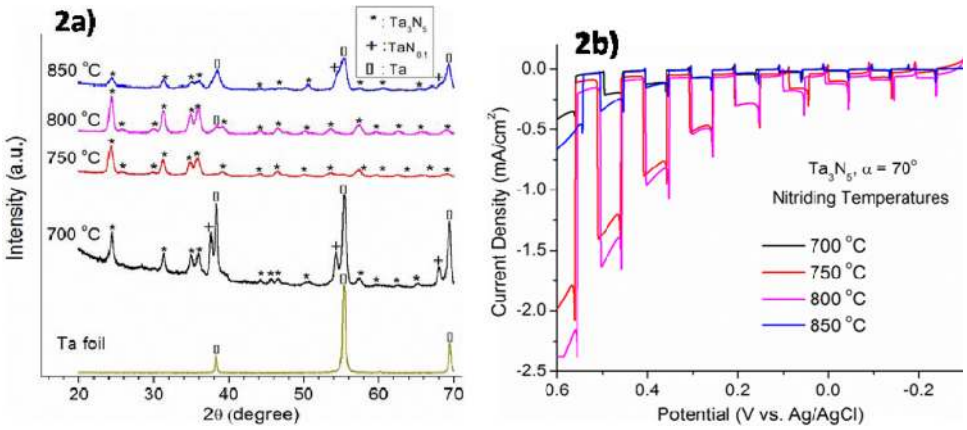

Figure 2. Ta_3N_5 films obtained at various nitriding temperatures. (a) XRD patterns (curves are offset) with a Ta substrate after nitridation included. (b) Chopped light PEC performance in 1 M KOH using full spectrum illumination (~73 mW/cm^2 xenon lamp).

3 in.-diameter quartz tube at the rate of 100 mL/min at a pressure slightly above atmospheric by bubbling the effluent gas flow through a water reservoir. Before the samples were heated, the tube furnace was purged with NH_3 for 1 h. The samples were then heated from room temperature to the desired annealing temperatures with a temperature ramp rate of 3 °C/min, and finally allowed to cool naturally after the desired nitridation duration was reached. The cobalt treatment was carried out by submerging Ta_3N_5 films in 0.1 M $Co(NO_3)_2$ (99.999% purity, Alfa Aesar) for ~10 min followed by rinsing with deionized water.

Film Characterization. XRD data were acquired with a Bruker D8 diffractometer using Cu Kα radiation (λ = 1.54 Å) with detector scan mode with an incident angle of 2° at a scan speed of 6 deg/min. SEM images were taken using a Zeiss FE-SEM at a 5 kV focus voltage. X-ray photoelectron spectroscopy (XPS) measurements were performed using a Kratos AXIS X-ray photoelectron spectrometer with Mono Al radiation. The atomic ratios were calculated using CasaXPS software with each element's relative sensitivity factors specific to the Kratos XPS. The diffuse reflectance spectroscopy (DRS) measurements were performed using a Varian Cary 500 UV−vis−NIR spectrophotometer with a Labsphere DR-CA-5500 intergrating sphere. The film absorptance was calculated from the corresponding reflectance by assuming that the sum of the film's reflectance and absorptance was 100%. High-resolution transmission electron microscopy (HRTEM) images were collected using a JEOL 2010F transmission electron microscope operated at 200 kV.

Photoelectrochemical Testing. A three-electrode electrochemical cell controlled by a potentiostat (CHI 660D, CH Instruments) was employed for PEC testing of the Ta_3N_5 films as photoanodes for water oxidation. The cell contained a Ag/AgCl reference electrode and a Pt wire counter electrode. The Ta_3N_5 film on the Ta substrate acted as the working electrode with an illuminated area of ~0.21 cm^2 exposed to an aqueous 1 M KOH solution, which was purged with N_2 gas for ~30 min prior to testing. Linear sweep voltammetry scans were obtained with a scan rate of 0.025 V/s from negative to positive potentials. Electrochemical impedance spectroscopy (EIS) measurements were carried out on a dense Ta_3N_5 film (the corresponding Ta_2O_5 film was deposited at normal incidence (α = 0°)) using the ideal semiconductor model[53] to obtain the Mott−Schottky plot at various frequencies. All electrochemical experiments were performed at room temperature. IPCE data were taken by employing a monochromator (Newport), and the light intensity at each selected wavelength was measured by an optical power meter (1916-C, Newport) equipped with a photodiode (818-UV, Newport). The following equation was used for calculating IPCE values:

$$\mathrm{IPCE} = [1240{*}i_p/(\lambda{*}E_\lambda)]{*}100\% \quad (1)$$

where i_p (μA) is the steady-state photocurrent and E_λ (μW) is the light power measured at the position of the film surface corresponding to a selected wavelength λ (nm). The spot of the incident light at the selected wavelength was adjusted to be within the O-ring area where the film was exposed to the 1 M KOH electrolyte. The overall applied-bias photon-to-current efficiency (ABPE)[54] (in 1 M KOH) was measured by using the two-electrode configuration cell with the Pt wire as the counter electrode and the Ta_3N_5 film as working electrode. The following equation was used for calculating ABPE values:

$$\mathrm{ABPE} = j_{ph}{*}(1.23 - V_{bias})/P_{total} \quad (2)$$

where j_{ph} (mA/cm^2) is the steady-state photocurrent density under the applied voltage V_{bias} (V) between the two electrodes (with a scan rate of 0.025 V/s from positive to negative potentials), and P_{total} (mW/cm^2) is the incident illumination power density. A xenon lamp (Newport) was utilized as the light source with a white-light intensity of ~73 mW/cm^2 measured by a thermopile detector with the spectrum response from 0.19 to 10.6 μm (Newport, 818P-020-12). A visible light cutoff filter (cutoff 420 nm, Newport) was employed to achieve visible light illumination.

Ring Collection/Substrate Generation Measurements. Scanning electrochemical microscopy (SECM) was used to measure the faradaic efficiency of the Ta_3N_5 films for water oxidation under irradiation.[50] A Au ring coated around an optical fiber (SFS200/200G, Fiberguide Industries, Inc., Long Hill, NJ) was used as a ring electrode.[55] The optical fiber has a diameter of 200 μm, and SiO_2 and Au were coated around the optical fiber with thicknesses of ~10 and 20 μm, respectively. The Au ring was coated with a borosilicate glass (capillary tubing, #27-32-1, FHC Inc., Bowdoin, ME) resulting in a final diameter of about 500 μm. Cyclic voltammetry (CV) of the ring (Figure S9a) shows the prepared electrode had no severe leakage, which is often observed for rings coated around the optical fiber. For the oxygen reduction reaction (ORR) at the ring, Pt was electrochemically deposited by repeated cyclic

dx.doi.org/10.1021/jp307369z | J. Phys. Chem. C 2012, 116, 19225−19232

voltammetry from 0.2 to −0.7 V for three cycles at a scan rate of 20 mV/s in a 10 mM H_2PtCl_6 and 0.1 M Na_2SO_4 aqueous solution. After the Pt deposition, distinctive hydrogen adsorption/desorption peaks appeared in the CV of the Pt plated Au ring (Figure S9b).

For the substrate generation/ring collection measurements, a SECM (model 900B, CH Instruments, Austin, TX) and a linear inchworm actuator (T-LA28A, Zaber Technologies Inc., Vancouver, Canada) were used. A Xe lamp (XBO 150 W, Osram, Munich, Germany) was used with the full output as a light source. Ferrocenemethanol (FcMeOH) (97%, Sigma-Aldrich), NaOH (97%, Fisher Scientific, Pittsburgh, PA), H_2PtCl_6 (99.9%, Alfa Aesar, Ward Hill, MA), and Na_2SO_4 (99.0%, Sigma-Aldrich, St. Louis, MO) were used as received.

RESULTS

Fabrication and Characterization of Ta_2O_5 Films by RBD. Figure 1a illustrates the preparation of Ta_2O_5 films by the RBD technique, and two typical types of morphologies of the as-deposited Ta_2O_5 films are presented in Figure 1b; both were grown in an ambient of 3×10^{-6} Torr O_2, but one was deposited at a glancing angle of 70° ($\alpha = 70°$), while the other was deposited at normal incidence ($\alpha = 0°$). Nanocolumnar structure is observed for the film deposited at $\alpha = 70°$, while a densely packed film without nanostructured features is seen for the deposition at $\alpha = 0°$. The as-deposited Ta_2O_5 films are amorphous as confirmed by using quartz substrates instead of Ta foils (Figure S1).

Nitriding Temperature Effects on PEC Performance. After deposition by RBD at 70° glancing incidence, 100 nm-thick Ta_2O_5 films were nitrided in a heated tube furnace filled with a 100 mL/min flow of NH_3 for 8 h at slightly above atmospheric pressure to convert the amorphous Ta_2O_5 to crystalline Ta_3N_5.

The X-ray diffraction (XRD) data shown in Figure 2a indicate that the Ta_3N_5 orthorhombic phase (PDF #01-072-0813) appears at 700 °C. This is a lower temperature than that reported earlier for converting micrometer-sized-Ta_2O_5 particles to Ta_3N_5 (850−900 °C).[17] However, our results are in agreement with earlier studies, suggesting that nanostructuring of the Ta_2O_5 films can assist in lowering the required nitriding temperature.[9,56] Over the temperature range 700−800 °C, Figure 2b shows the photoactivity of the Ta_3N_5 films increased with increasing temperature, probably due to the effectiveness of higher annealing temperatures in the conversion of Ta_2O_5 ($E_g \approx 4.0$ eV[57]) into crystallized Ta_3N_5 ($E_g \approx 2.1$ eV[3,57]), which has higher photocatalytic activity in the visible region. The films nitrided at 800 °C have the highest photocurrents over the investigated temperature range (700−850 °C), reaching 1.4 mA/cm^2 at +0.5 V vs Ag/AgCl (pH 13.6) or +1.5 V vs RHE (reversible hydrogen electrode). In Figure 2a, films nitrided at 850 °C have significant peaks assigned to tantalum metal. We hypothesize that at high temperature the decomposition of NH_3 to H_2 and N_2[11,58] is sufficiently rapid that during the nitridation process H_2 from the NH_3 decomposition at high temperature acts to reduce Ta^{5+} on the surface of Ta_2O_5 or Ta_3N_5 to lower oxidation states (such as those found in Ta or $TaN_{0.1}$). The failure to obtain a well-crystallized Ta_3N_5 phase employing an 850 °C nitridation temperature resulted in a lower photocatalytic activity as compared to similar films nitrided at 750 and 800 °C. Typical morphologies for dense and nanoporous Ta_3N_5 films prepared at various nitriding temperatures and a high-resolution transmission electron microscopy image of a Ta_2O_5 film after 800 °C nitridation are shown in Figures S1, S2. Longer nitridation at 700 and 800 °C (15 h instead of 8 h) was also investigated (Figures S3, S4), and thus nitridation at 800 °C for 8 h was chosen as optimal condition for further analysis.

To better understand the photocatalytic improvement of nanoporous Ta_3N_5 films as compared to densely packed ones, two Ta_3N_5 films were prepared at the same deposition (100 nm thickness) and nitridation conditions (800 °C, 8 h) except for deposition angle during Ta_2O_5 deposition: one film was deposited at $\alpha = 0°$ to produce a dense film and the other at $\alpha = 70°$ to produce a nanoporous film. In similar PEC tests, the Ta_3N_5 porous film had a photocurrent ~3 times higher than the dense film (Figure 3a). As compared to a dense film of the same thickness, the nanoporous film has a more open structure that increases the likelihood of the photogenerated holes reaching the solid−liquid interface (shorter transport pathway) rather than recombining with the electrons within the bulk film, which benefits the PEC performance. The contribution from the visible portion of the whole spectrum for a 100 nm nanoporous Ta_3N_5 film is estimated to be ~80% by calculating the ratio between the steady-state photocurrent value from the visible region and from the whole spectrum (white-light illumination) (Figure 3b).

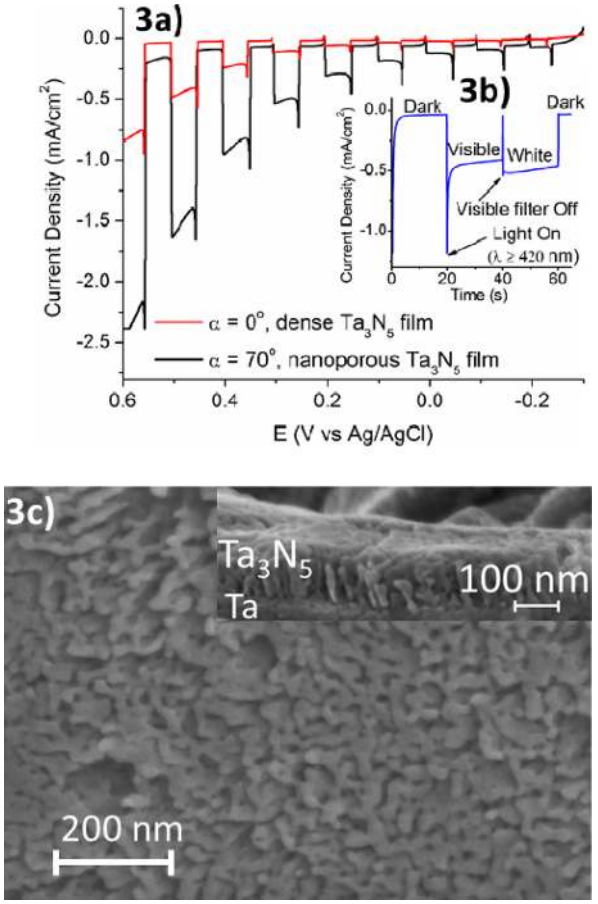

Figure 3. (a) Chopped light experiments using full spectrum illumination (~73 mW/cm^2 xenon lamp) in 1 M KOH for 100 nm nanoporous and dense Ta_3N_5 films. (b) Chronoamperometry of the nanoporous film under 0.5 V vs Ag/AgCl. (c) Top view and cross-sectional (inset) SEM images of the nanoporous Ta_3N_5 film.

dx.doi.org/10.1021/jp307369z | J. Phys. Chem. C 2012, 116, 19225−19232

The Ta_3N_5 film thickness was estimated from a cross-sectional scanning electron microscopy (SEM) image of a Ta_3N_5 film prepared at 800 °C (Figure 3c) to be ∼100 nm, essentially the same as the original RBD Ta_2O_5 film. This result is somewhat consistent with earlier studies on the pseudomorphic transformation of Ta_2O_5 into Ta_3N_5[7] although the feathery structure of RBD Ta_2O_5 is lost after the nitridation process. It is also observed that only the Ta_2O_5 layer was nitrided and not the Ta substrate underneath.[3,8] This confirms the advantage of using Ta foils as stable substrates for the synthesis of nanostructured Ta_3N_5 films as well as their utility as an electrical contact for the Ta_3N_5 electrodes for PEC applications.

A Mott−Schottky (MS) plot (Figure 4) was obtained by EIS measurements using frequencies ranging from 500 to 3000 Hz

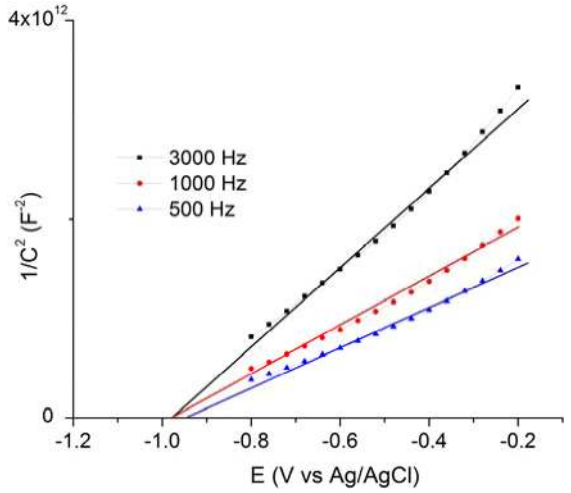

Figure 4. MS plots derived from EIS performed at various frequencies in 1 M KOH for a 100 nm dense Ta_3N_5 film.

in 1 M KOH (pH = 13.6). In this case, a dense film was used to more accurately represent the planar electrode assumed by the model RC circuit to generate the MS plots from the impedance data. The MS plot confirms the n-type behavior of Ta_3N_5 semiconductor electrodes. By taking the intercept between the linear fit to the MS plot and the potential axis, the flat band potential (E_{fb}) of our Ta_3N_5 films was estimated to be ∼ −1.05 V vs Ag/AgCl or ∼ −0.85 V vs NHE at pH = 13.6.

A light chopping experiment near this potential was also carried out to estimate the transient photoanodic current onset potential of this Ta_3N_5 film, and a similar value was obtained (Figure S7). This finding is consistent with earlier studies reporting the flat band potential of Ta_3N_5 films and confirms that the conduction band edge of Ta_3N_5 is more negative than the proton reduction potential (∼ −0.8 V vs NHE) at pH 13.6,[8,57] making Ta_3N_5 a theoretically possible material for an unbiased, single PEC water splitting system. However, Figure 2b showed the photocurrent is negligible at ∼ −0.3 V vs Ag/AgCl, suggesting that in fact few electrons are produced at potentials for water reduction.

Ta_3N_5 Film's Photocorrosion and the Cobalt Surface Treatment To Improve the Photostability. Figure 3b (and later Figure 7a) indicates the fresh Ta_3N_5 electrode undergoes significant degradation under illumination in 1 M KOH despite its high initial photocurrent. This photocorrosion can be explained by the oxidation of the nitrogen anions on the electrode surface to N_2 by photogenerated holes during the course of light illumination as is often found with oxynitrides with d^0 electronic configuration, for which a small amount of gaseous N_2 can be observed during the initial portions of photocatalytic tests.[59] In comparing the Ta_3N_5 and Ta_2O_5 band edge positions,[57] the conduction band (CB) of Ta5d orbitals is unchanged; however, the valence band (VB) position of Ta_3N_5 (the top of the VB is the N2p orbital, $E_{VB} \approx 1.58$ V vs NHE at pH = 0) is much closer to the water oxidation potential than the VB of Ta_2O_5 (the top of the VB is the O2p orbital, $E_{VB} \approx$ 3.39 V vs NHE at pH = 0). As photogenerated holes are trapped at the VB edge, the more negative (on an electrochemical scale) VB of Ta_3N_5 as compared to Ta_2O_5 results in a decrease in the holes' oxidation power, making the water oxidation reaction less preferred,[60] leading to photocorrosion of the film instead. A dark scan of a typical Ta_3N_5 film (Figure S8) shows the oxidation of the Ta_3N_5 film happens at a lower potential than the thermodynamic onset potential for the oxidation of water. This implies that photocorrosion will occur unless the water oxidation reaction is made much more favorable kinetically.

XPS measurements were carried out to investigate the surface composition and chemical nature of the Ta_3N_5 films (all nitrided at 800 °C for 8 h) before and after PEC testing. Two areas of the same Ta_3N_5 film were analyzed, one with and the

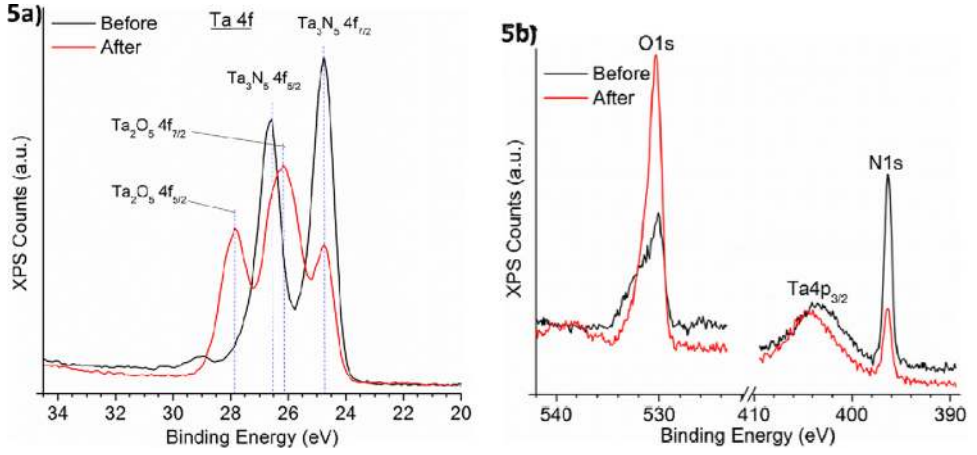

Figure 5. XPS spectra of a Ta_3N_5 film before and after full spectrum illumination for 30 min in 1 M KOH at +0.5 V vs Ag/AgCl. (a) Ta4f ; (b) O1s, Ta4p, N1s. The corresponding Ta_2O_5 film was 100 nm thick and grown at 70° deposition angle by RBD prior to nitridation.

dx.doi.org/10.1021/jp307369z | J. Phys. Chem. C 2012, 116, 19225−19232

other without exposure to the full spectrum of a xenon lamp (~73 mW/cm^2) for 30 min in 1 M KOH at +0.5 V vs Ag/AgCl (Figure 5).

The binding energies were calibrated by using the contaminating carbon C1s peak at 284.5 eV as a standard. In Figure 5a, the original Ta_3N_5 film has $Ta4f_{7/2}$ and $Ta4f_{5/2}$ features, which are assigned to Ta^{5+} in Ta_3N_5,[3,57] while the film after light illumination has $Ta4f_{7/2}$ and $Ta4f_{5/2}$ peaks at 27.8 and 26.2 eV, respectively, corresponding to Ta^{5+} in Ta_2O_5.[57,61] Also, after illumination, the $Ta4f_{7/2}$ peak (at 24.7 eV, assigned to Ta_3N_5) remained but showed lower intensity. In Figure 5b, the intensity of the O1s peak increased after illumination while the intensity of the N1s peak decreased. The changes in XPS spectra as well as the change of atomic ratios (O/Ta increased while N/Ta decreased (Table 1)), all indicate the oxidation of the Ta_3N_5 electrode surface by photogenerated holes[3,8] under light irradiation:

$$2Ta_3N_5 + 30h^+ + 30OH^- \rightarrow 3Ta_2O_5 + 5N_2 + 15H_2O$$

The PEC performance improvement and suppression of the oxidation of Ta_3N_5 films under illumination has been studied by loading IrO_2[3] or Pt[12] as electrocatalysts. Recently, the use of cobalt-based eletrocatalysts to improve the PEC performance of various photoanodes has been given attention because cobalt is inexpensive and abundant.[45−52] In a study by Kay at el.[46] regarding a cobalt surface treatment of α-Fe_2O_3, Co^{2+} was adsorbed on the Fe_2O_3 electrode by simply submerging the electrode in a dilute $Co(NO_3)_2$ aqueous solution.

Table 1. Atomic Ratios of O/Ta, N/Ta, and Co/Ta on the Cobalt-Treated Ta_3N_5 Film Surface before and after Full-Spectrum Light Irradiation (~73 mW/cm^2) for 30 min at +0.5 V vs Ag/AgCl in 1 M KOH

XPS measurement on film surface	atomic ratios	O/Ta	N/Ta	Co/Ta
untreated Ta_3N_5 films	before	1.27	1.23	
	after 30 min illumination	2.08	0.42	
cobalt-treated Ta_3N_5 films	before	1.50	1.92	0.42
	after 30 min illumination	2.09	1.26	0.22

Here, we attempted a similar approach; Co^{2+} was adsorbed on the film surface by submerging the fresh Ta_3N_5 films in a 0.1 M $Co(NO_3)_2$ solution for ~10 min followed by rinsing with deionized water prior to PEC testing. Figure 6a illustrates the improved stability of the cobalt-treated Ta_3N_5 film under visible illumination. The existence of transient spikes during intermittent illumination has also been observed for Fe_2O_3 films and can be a result of recombination or the back reaction of photogenerated species (oxy or hydroxyl) on the surface.[62−64] Although the current drops slightly over time, the photocurrent remains clearly higher than that of the untreated Ta_3N_5 film. This behavior is consistent with the result for the cobalt treatment of α-Fe_2O_3[46] and suggests that the surface cobalt sites facilitate the water oxidation reaction and inhibit to some extent the film's self-oxidation by photogenerated holes. For the same reason, higher, more stable photocurrents of the cobalt-treated Ta_3N_5 films resulted in an IPCE enhancement (Figure 6b). Diffuse reflectance spectroscopy measurements are shown in Figure 6c in which the onset wavelength of the film is ~620 nm indicating $E_g \approx 2.0$ eV. This value is in agreement with earlier studies[3,9] and also with the onset wavelength from IPCE measurements (Figure 6b) and that of pristine Ta_3N_5 photoanodes for water oxidation (Figure S5). These IPCE values are similar to those observed by Feng et al.[9] for Ta_3N_5 nanotubes. Since stability was not discussed in their work, those values may represent the initial high performance of the films prior to degradation. The applied-bias photon-to-current efficiency (ABPE) was measured to calculate our cell's overall solar energy efficiency using a two-electrode configuration in 1 M KOH. The ABPE values at 0.5 V vs a Pt counter electrode for 100 nm-thick nanoporous Ta_3N_5 films before and after the cobalt loading are 0.04% and 0.24%, illustrating the enhancement of the overall PEC performance by the cobalt treatment.

As shown in Table 1, on the cobalt-treated Ta_3N_5 film after illumination the O content increased by 39%, while the N content decreased by 34% as compared to the values of 64% and 67%, respectively, for the untreated Ta_3N_5 films. This comparison suggests the suppression of Ta_3N_5 oxidation by the adsorbed cobalt on the film surface. The cobalt content of the treated films decreased after PEC testing, which might be due to the removal of some excess cobalt during testing or the instability of the cobalt on the surface of the film as mentioned earlier in the study involving the cobalt-treated hematite

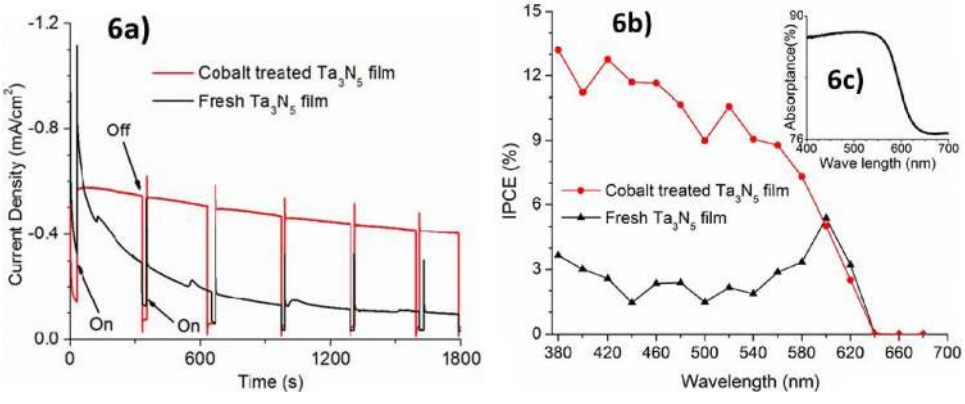

Figure 6. (a) Amperometric i−t curve for nanoporous Ta_3N_5 films with and without cobalt treatment in 1 M KOH at +0.5 V vs Ag/AgCl under visible illumination. (b) IPCE comparison of Ta_3N_5 films with and without cobalt surface treatment in 1 M KOH at +0.2 V vs Ag/AgCl. (c) Absorptance spectrum calculated from the diffuse reflectance of a Ta_3N_5 film on Ta foil. The corresponding Ta_2O_5 films were 100 nm thick and grown at 70° deposition angle by RBD prior to nitridation. The light source is a ~73 mW/cm^2 xenon lamp.

dx.doi.org/10.1021/jp307369z | J. Phys. Chem. C 2012, 116, 19225−19232

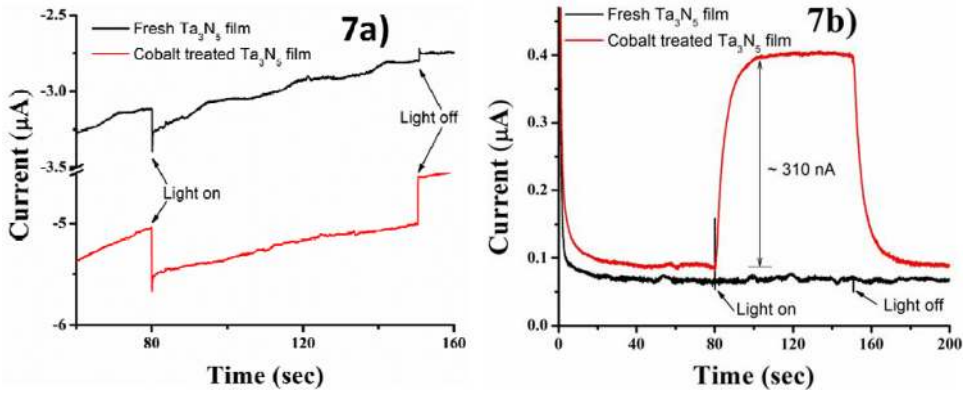

Figure 7. (a) Photooxidation current of 100 nm nanoporous Ta_3N_5 films measured in 0.1 M NaOH at 0.5 V vs Ag/AgCl. The UV−visible irradiation was switched on from 80 to 150 s. (b) Collected current at the Pt RDE tip electrode 30 μm above the Ta_3N_5 films. The tip electrode was held at −0.4 V vs Ag/AgCl for the diffusion limited ORR.

photoanode.[47] We note that the current cobalt treatment may be not the final solution for the instability issue; further investigation is needed regarding how to load stable eletrocatalysts on the Ta_3N_5 surface. Recently, two studies have appeared reporting on the stability and PEC enhancement of Ta_3N_5 films by the loading of Co_3O_4 via immersing the films in either Co_3O_4 nanoparticles[55] or $Co(OH)_x$ colloidal solutions followed by 300 °C calcination in air.[52] The presence of Co^{2+} on our cobalt-treated Ta_3N_5 film is shown in Figure S8.

To further study the Ta_3N_5 films' photocorrosion, scanning electrochemical microscopy (SECM) was employed to ascertain the origin of the current generated from Ta_3N_5 photoanodes (i.e., water oxidation versus photocorrosion). Details of the experimental setup can be found in the Experimental Section. Briefly, during illumination a fiber optic with a platinum-plated Au ring was placed 30 μm above the Ta_3N_5 films to detect generated oxygen by measuring the current at the ring corresponding to the oxygen reduction reaction (ORR). When this current is compared to the oxidation current measured at the Ta_3N_5 anode, a collection efficiency can be calculated. The collection efficiency is defined as the ratio of the ring current (collection) and the photo-oxidation current (generation).

As shown in Figure 7a, a photo-oxidation current at the cobalt-treated nanoporous Ta_3N_5 film held stable at ~470 nA at 0.5 V vs Ag/AgCl. The estimated current density based on the irradiation area (4×10^{-4} cm^2) was ~1 mA/cm^2, on the same order as that shown in Figure 2b. The photo-oxidation current from the untreated Ta_3N_5 film decreased from 150 to 60 nA, while the current collected at the ring electrode was near zero (indicating little or no oxygen evolution). However, for the cobalt-treated film, the generation current was 470 nA, and the collection current was ~310 nA. The overall collection efficiency was thus calculated to be 67% for the cobalt-treated film, where the theoretical maximum collection efficiency (for a tip−substrate distance of 30 μm) was determined to be 87%.[55] Thus, the faradaic efficiency of the cobalt-treated nanoporous Ta_3N_5 electrode for water oxidation is ~77%.

CONCLUSIONS

Nanostructured Ta_3N_5 films have been prepared via reactive ballistic deposition (RBD) followed by a nitridation step over a temperature range of 700−850 °C, for which Ta_3N_5 films nitrided at 800 °C showed the highest photocurrents in 1 M KOH. The photocatalytic activity of a nanoporous Ta_3N_5 film prepared at a 70° glancing angle is 3 times higher than a dense film of similar thickness, confirming the advantage of using nanostructured Ta_3N_5 for photoelectrochemical water oxidation. Additionally, XPS measurements revealed that the degradation of Ta_3N_5 films during water oxidation testing is from the film's oxidation by photogenerated holes. SECM measurements found a faradaic efficiency for water oxidation of ~77% for cobalt-treated 100 nm nanostructured Ta_3N_5 film, confirming the suppression of the films' photocorrosion by this simple cobalt surface treatment.

ASSOCIATED CONTENT

Supporting Information

Details of experimental methods, XRD patterns, and the PEC performance of Ta_3N_5 films nitrided for 15 h, IPCE measurements, estimation of onset potential, a dark scan of a Ta_3N_5 film, and XPS spectra as indicated in the text, as well as cyclic voltammograms of the tip electrodes used in the SECM measurements. This material is available free of charge via the Internet at http://pubs.acs.org.

AUTHOR INFORMATION

Corresponding Author

*E-mail: mullins@che.utexas.edu.

Notes

The authors declare no competing financial interest.

ACKNOWLEDGMENTS

C.B.M. and A.J.B. gratefully acknowledge the support of the National Science Foundation (CHE-0934450). C.B.M. and A.J.B. also acknowledge the Welch Foundation (C.B.M., F-1436; and A.J.B., F-0021) for their generous support. C.B.M. and A.J.B. also acknowledge the National Science Foundation (Grant No. 0618242) for funding the X-ray photoelectron spectrometer and the Kratos AXIS Ultra DLD spectrometer used in this work. H.X.D. thanks Vincent C. Holmberg for help regarding DRS measurements. Finally, H.X.D. thanks the Vietnam Education Foundation (VEF) for a graduate fellowship.

REFERENCES

(1) Kamat, P. V. *J. Phys. Chem. C* **2007**, *111*, 2834−2860.
(2) Bard, A. J.; Fox, M. A. *Acc. Chem. Res.* **1995**, *28*, 141−145.

(3) Yokoyama, D.; Hashiguchi, H.; Maeda, K.; Minegishi, T.; Takata, T.; Abe, R.; Kubota, J.; Domen, K. *Thin Solid Films* **2010**, *519*, 2087−2092.
(4) Fujishima, A.; Honda, K. *Nature* **1972**, *238*, 37−38.
(5) Hara, M.; Chiba, E.; Ishikawa, A.; Takata, T.; Kondo, J. N.; Domen, K. *J. Phys. Chem. B* **2003**, *107*, 13441−13445.
(6) Tabata, M.; Maeda, K.; Higashi, M.; Lu, D.; Takata, T.; Abe, R.; Domen, K. *Langmuir* **2010**, *26*, 9161−9165.
(7) Lu, D.; Hitoki, G.; Katou, E.; Kondo, J. N.; Hara, M.; Domen, K. *Chem. Mater.* **2004**, *16*, 1603−1605.
(8) Ishikawa, A.; Takata, T.; Kondo, J. N.; Hara, M.; Domen, K. *J. Phys. Chem. B* **2004**, *108*, 11049−11053.
(9) Feng, X.; LaTempa, T. J.; Basham, J. I.; Mor, G. K.; Varghese, O. K.; Grimes, C. A. *Nano Lett.* **2010**, *10*, 948−952.
(10) Murphy, A. B.; Barnes, P. R. F.; Randeniya, L. K.; Plumb, I. C.; Grey, I. E.; Horne, M. D.; Glasscock, J. A. *Int. J. Hydrogen Energy* **2006**, *31*, 1999−2017.
(11) Lee, Y.; Nukumizu, K.; Watanabe, T.; Takata, T.; Hara, M.; Yoshimura, M.; Domen, K. *Chem. Lett.* **2006**, *35*, 352−353.
(12) Yuliati, L.; Yang, J.-H.; Wang, X.; Maeda, K.; Takata, T.; Antonietti, M.; Domen, K. *J. Mater. Chem.* **2010**, *20*, 4295−4298.
(13) Hitoki, G.; Takata, T.; Kondo, J. N.; Hara, M.; Kobayashi, H.; Domen, K. *Chem. Commun.* **2002**, 1698−1699.
(14) Ho, C.-T.; Low, K.-B.; Klie, R. F.; Maeda, K.; Domen, K.; Meyer, R. J.; Snee, P. T. *J. Phys. Chem. C* **2011**, *115*, 647−652.
(15) Ho, C.-T.; Low, K.-B.; Jash, P.; Shen, H.; Snee, P. T.; Meyer, R. J. *Chem. Mater.* **2011**, *23*, 4721−4725.
(16) Higashi, M.; Domen, K.; Abe, R. *Energy Environ. Sci.* **2011**, *4*, 4138−4147.
(17) Hitoki, G.; Ishikawa, A.; Takata, T.; Kondo, J. N.; Hara, M.; Domen, K. *Chem. Lett.* **2002**, *31*, 736−737.
(18) Family, F. *J. Stat. Phys.* **1996**, *83*, 1255−1259.
(19) Abelmann, L.; Lodder, C. *Thin Solid Films* **1997**, *305*, 1−21.
(20) Robbie, K.; Sit, J. C.; Brett, M. J. *J. Vac. Sci. Technol., B* **1998**, *16*, 1115−1122.
(21) Hawkeye, M. M.; Brett, M. J. *J. Vac. Sci. Technol., A* **2007**, *25*, 1317−1335.
(22) Dohnálek, Z.; Kimmel, G. A.; McCready, D. E.; Young, J. S.; Dohnálková, A.; Smith, R. S.; Kay, B. D. *J. Phys. Chem. B* **2002**, *106*, 3526−3529.
(23) Flaherty, D. W.; Hahn, N. T.; May, R. A.; Berglund, S. P.; Lin, Y.-M.; Stevenson, K. J.; Dohnalek, Z.; Kay, B. D.; Mullins, C. B. *Acc. Chem. Res.* **2012**, *45*, 434−443.
(24) Kim, J.; Dohnálek, Z.; Kay, B. D. *Surf. Sci.* **2005**, *586*, 137−145.
(25) Robbie, K.; Friedrich, L. J.; Dew, S. K.; Smy, T.; Brett, M. J. *J. Vac. Sci. Technol., A* **1995**, *13*, 1032−1035.
(26) Liu, F.; Umlor, M. T.; Shen, L.; Weston, J.; Eads, W.; Barnard, J. A.; Mankey, G. J. *J. Appl. Phys.* **1999**, *85*, 5486−5488.
(27) Sit, J. C.; Vick, D.; Robbie, K.; Brett, M. J. *J. Mater. Res.* **1999**, *14*, 1197−1199.
(28) Krause, K. M.; Taschuk, M. T.; Harris, K. D.; Rider, D. A.; Wakefield, N. G.; Sit, J. C.; Buriak, J. M.; Thommes, M.; Brett, M. J. *Langmuir* **2009**, *26*, 4368−4376.
(29) Colgan, M. J.; Djurfors, B.; Ivey, D. G.; Brett, M. J. *Thin Solid Films* **2004**, *466*, 92−96.
(30) Flaherty, D. W.; Dohnálek, Z.; Dohnálková, A.; Arey, B. W.; McCready, D. E.; Ponnusamy, N.; Mullins, C. B.; Kay, B. D. *J. Phys. Chem. C* **2007**, *111*, 4765−4773.
(31) Lin, Y.-M.; Abel, P. R.; Flaherty, D. W.; Wu, J.; Stevenson, K. J.; Heller, A.; Mullins, C. B. *J. Phys. Chem. C* **2011**, *115*, 2585−2591.
(32) Robbie, K.; Brett, M. J.; Lakhtakia, A. *Nature* **1996**, *384*, 616−616.
(33) Motohiro, T.; Taga, Y. *Appl. Opt.* **1989**, *28*, 2466−2482.
(34) Rico, V.; Borrsás, A.; Yubero, F.; Espinós, J. P.; Frutos, F.; González-Elipe, A. R. *J. Phys. Chem. C* **2009**, *113*, 3775−3784.
(35) Messier, R.; Venugopal, V. C.; Sunal, P. D. Origin and evolution of sculptured thin films. The 46th international symposium of the American Vacuum Society, 2000.
(36) Seto, M. W.; Robbie, K.; Vick, D.; Brett, M. J.; Kuhn, L. *J. Vac. Sci. Technol., B* **1999**, *17*, 2172−2177.
(37) Flaherty, D. W.; Hahn, N. T.; Ferrer, D.; Engstrom, T. R.; Tanaka, P. L.; Mullins, C. B. *J. Phys. Chem. C* **2009**, *113*, 12742−12752.
(38) Flaherty, D. W.; May, R. A.; Berglund, S. P.; Stevenson, K. J.; Mullins, C. B. *Chem. Mater.* **2009**, *22*, 319−329.
(39) May, R. A.; Flaherty, D. W.; Mullins, C. B.; Stevenson, K. J. *J. Phys. Chem. Lett.* **2010**, *1*, 1264−1268.
(40) Hahn, N. T.; Ye, H.; Flaherty, D. W.; Bard, A. J.; Mullins, C. B. *ACS Nano* **2010**, *4*, 1977−1986.
(41) Hahn, N. T.; Mullins, C. B. *Chem. Mater.* **2010**, *22*, 6474−6482.
(42) Chemelewski, W. D.; Hahn, N. T.; Mullins, C. B. *J. Phys. Chem. C* **2012**, *116*, 5255−5261.
(43) Berglund, S. P.; Flaherty, D. W.; Hahn, N. T.; Bard, A. J.; Mullins, C. B. *J. Phys. Chem. C* **2011**, *115*, 3794−3802.
(44) Berglund, S. P.; Rettie, A. J. E.; Hoang, S.; Mullins, C. B. *Phys. Chem. Chem. Phys.* **2012**, *14*, 7065−7075.
(45) Kanan, M. W.; Nocera, D. G. *Science* **2008**, *321*, 1072−1075.
(46) Kay, A.; Cesar, I.; Gratzel, M. *J. Am. Chem. Soc.* **2006**, *128*, 15714−15721.
(47) Barroso, M.; Cowan, A. J.; Pendlebury, S. R.; Gratzel, M.; Klug, D. R.; Durrant, J. R. *J. Am. Chem. Soc.* **2011**, *133*, 14868−14871.
(48) McDonald, K. J.; Choi, K.-S. *Chem. Mater.* **2011**, *23*, 1686−1693.
(49) Seabold, J. A.; Choi, K.-S. *Chem. Mater.* **2011**, *23*, 1105−1112.
(50) Ye, H.; Park, H. S.; Bard, A. J. *J. Phys. Chem. C* **2011**, *115*, 12464−12470.
(51) Cong, Y.; Park, H. S.; Dang, H. X.; Fan, F.-R. F.; Bard, A. J.; Mullins, C. B. *Chem. Mater.* **2012**, *24*, 579−586.
(52) Liao, M.; Feng, J.; Luo, W.; Wang, Z.; Zhang, J.; Li, Z.; Yu, T.; Zou, Z. *Adv. Funct. Mater.* **2012**, *22*, 3066−3074.
(53) Bard, A.; Faulkner, L. *Electrochemical Methods: Fundamentals and Applications*, 2nd ed.; John Wiley & Sons, Inc.: New York, 2001.
(54) Chen, Z.; Jaramillo, T. F.; Deutsch, T. G.; Kleiman-Shwarsctein, A.; Forman, A. J.; Gaillard, N.; Garland, R.; Takanabe, K.; Heske, C.; Sunkara, M.; et al. *J. Mater. Res.* **2010**, *25*, 3−16.
(55) Cong, Y.; Park, H. S.; Wang, S.; Dang, H. X.; Fan, F.-R. F.; Mullins, C. B.; Bard, A. J. *J. Phys. Chem. C* **2012**, *116*, 14541−14550.
(56) Banerjee, S.; Mohapatra, S. K.; Misra, M. *Chem. Commun.* **2009**, 7137−7139.
(57) Chun, W.-J.; Ishikawa, A.; Fujisawa, H.; Takata, T.; Kondo, J. N.; Hara, M.; Kawai, M.; Matsumoto, Y.; Domen, K. *J. Phys. Chem. B* **2003**, *107*, 1798−1803.
(58) Maeda, K.; Terashima, H.; Kase, K.; Higashi, M.; Tabata, M.; Domen, K. *Bull. Chem. Soc. Jpn.* **2008**, *81*, 927−937.
(59) Maeda, K.; Domen, K. *MRS Bull.* **2011**, *36*, 25−31.
(60) Nakamura, R.; Tanaka, T.; Nakato, Y. *J. Phys. Chem. B* **2005**, *109*, 8920−8927.
(61) Kerrec, O.; Devilliers, D.; Groult, H.; Marcus, P. *Mater. Sci. Eng., B* **1998**, *55*, 134−142.
(62) Hardee, K. L.; Bard, A. J. *J. Electrochem. Soc.* **1977**, *124*, 215−224.
(63) Iwanski, P.; Curran, J. S.; Gissler, W.; Memming, R. *J. Electrochem. Soc.* **1981**, *128*, 2128−2133.
(64) Anderman, M.; Kennedy, J. H. *J. Electrochem. Soc.* **1984**, *131*, 21−26.